Available online at www.sciencedirect.com
SCIENCE DIRECT®
International Journal of Heat and Fluid Flow 24 (2003) 29–40
International Journal of HEAT AND FLUID FLOW
www.elsevier.com/locate/ijhff

Development of a nonlinear near-wall turbulence model for turbulent flow and heat transfer

Tae Seon Park [a], Hyung Jin Sung [b,*], Kenjiro Suzuki [c]

[a] *Rocket Engine Research Development, Korea Aerospace Research Institute, 45 Oun-dong, Yusong-ku, Taejon 305-333, South Korea*
[b] *Department of Mechanical Engineering, Korea Advanced Institute of Science and Technology, 373-1 Kusong-dong, Yusong-ku, Taejon 305-701, South Korea*
[c] *Department of Mechanical Engineering, Kyoto University, Kyoto 606-8501, Japan*

Received 13 November 2001; accepted 30 July 2002

Abstract

A new nonlinear near-wall turbulence model is developed on the basis of realizability constraints to predict turbulent flow and heat transfer in strongly nonequilibrium flows. The linear k–ε–f_μ model of Park and Sung (Fluid Dyn. Res., 20 (1997) 97) is extended to a nonlinear formulation. The stress–strain relationship is derived from the Cayley–Hamilton theorem in a homogeneous flow. The ratio of production to dissipation (P_k/ε) is employed to solve an algebraic equation of the strain dependent coefficients. A near-wall treatment is dealt with by reproducing the model coefficients from a modified strain variable. An improved explicit heat flux model is proposed with the aid of Cayley–Hamilton theorem, which includes the quadratic effects of flow deformations. The near-wall asymptotic behavior is incorporated by modifying the f_λ function. Emphasis is placed on the model performance on the truncated strain terms. The model performance is shown to be generally satisfactory.

Keywords: Turbulence modeling; Nonlinear k–ε–f_μ model; Explicit heat flux model

1. Introduction

Near-wall behaviors of velocity and temperature are of prime importance in predicting accurate momentum and heat transfer in the vicinity of the wall. Turbulence quantities close to the wall are strongly anisotropic because the turbulent velocity fluctuations normal to the wall are damped by the presence of the wall. It is known that the linear eddy-viscosity models show some deficiencies in the prediction of the anisotropic characteristics. These include an inability to capture the normal stress anisotropy, insufficient sensitivity to the secondary strains, seriously excessive generation of turbulence at the impinging regions, and violation of the realizability at large rates of strain. These deficiencies may be attributed to the fact that the constitutive relation of the deviatoric Reynolds stress tensor is assumed to be linear to the local mean strain (Apsley and Leschziner, 1998; Craft et al., 1996; Gatski and Speziale, 1993; Park and Sung, 1995; Wallin and Johansson, 2000).

In order to incorporate the anisotropic effects into turbulence modelings, many versions of the explicit algebraic stress models (EASMs) have been developed by extending them into a nonlinear fashion of the linear models (Apsley and Leschziner, 1998; Craft et al., 1996; Gatski and Speziale, 1993; Park and Sung, 1995; Wallin and Johansson, 2000). The models are generally expressed by the quadratic or cubic relations in mean velocity gradients. It is known that the quadratic and cubic terms contribute to the normal stress anisotropy. However, the anisotropic characteristics in the near-wall region have not been well reproduced by these models. In the present study, a new nonlinear model is developed on the basis of the linear k–ε–f_μ model of Park and Sung (1997). The nonlinear formulation is derived from the Cayley–Hamilton theorem (Pope, 1975) in a homogeneous flow. The coefficients of various nonlinear terms are determined from Schwarz' inequality and realizability constraints. To resolve the near-wall anisotropy, the nonlinear terms are modified by additional coefficients

* Corresponding author. Tel.: +82-42-869-3027; fax: +82-42-869-5027.
E-mail address: hjsung@kaist.ac.kr (H.J. Sung).

0142-727X/02/$ - see front matter © 2002 Elsevier Science Inc. All rights reserved.
PII: S0142-727X(02)00211-4

Nomenclature

b_{ij}	anisotropy tensor, $\overline{u_iu_j}/2k - \delta_{ij}/3$
C_f	skin friction coefficient
C_μ, $C_{\varepsilon1}$, $C_{\varepsilon2}$	model constants
D	jet diameter
ER	expansion ratio of backward-facing step
f_μ, f_2, f_λ	model functions
H	jet-to-wall distance
H_b	height of backward-facing step
k	turbulent kinetic energy
k_f	thermal conductivity
Nu	Nusselt number, $Nu = hD/k_f$
Pr	Prandtl number, $Pr = \nu/\alpha$
Pr_t	turbulent Prandtl number
q_w	constant surface heat flux
r	radial distance
R_t	turbulent Reynolds number, $k^2/\nu\varepsilon$
Re_D	Reynolds number, $Re_D = U_bD/\nu$
Re_H	Reynolds number, $Re_H = U_oH_b/\nu$
S_{ij}	strain rate tensor, $S_{ij} = 0.5(U_{i,j} + U_{j,i})$
T_K	Kolmogorov timescale, $\sqrt{\nu/\varepsilon}$
W_{ij}	vorticity tensor, $W_{ij} = 0.5(U_{i,j} - U_{j,i})$
St	Stanton number, $St = q_w/(\rho C_pU_o)/(T_w - T_{ref})$
T	mean temperature
T_{ref}	reference mean temperature
T_w	wall temperature
U	mean velocity
U_b	jet bulk velocity
U_o	reference mean velocity
y	wall coordinate
Greeks	
α_t	thermal eddy diffusivity
β_i	coefficients of nonlinear stress–strain relation
δ_{ij}	Kronecker delta
γ_i	coefficients of nonlinear heat flux model
ε	dissipation rate of turbulent energy
ν	kinematic molecular viscosity
ν_t	eddy viscosity
τ_{ij}	Reynolds stress, $\overline{u_iu_j}$
θ	fluctuating temperature

of the strain variables. These terms behave as a damping function similar to the low-Reynolds number models. In order to see the effect of strain dependent terms, the model performance is examined with the truncated nonlinear relation. The resulting near-wall behaviors are then calibrated with the available DNS data. The present nonlinear model is validated by predicting several turbulent flows, e.g. channel, backward-facing step and impinging jet flows.

On the basis of the nonlinear model, an explicit turbulent heat flux model is derived in the present study. In general, the turbulent heat transfer is solved with the Boussinesq approximation. The unknown heat flux is then calculated by prescribing the value of a constant turbulent Prandtl number Pr_t, which satisfies Pope's linear principle of scalars in turbulent flows. However, this approach is not adequate to predict convective heat transfer in separated and reattaching flows (Rhee and Sung, 2000). This is because the constant Pr_t assumption is no longer applicable to the anisotropy of turbulent scalar flux. Recently, Rhee and Sung (2000) developed a nonlinear heat transfer model for turbulent separated and reattaching flows. However, the effect of large strains is not fully taken into consideration. In the present study, a nonlinear heat flux model is developed including the effect of large strains. An explicit algebraic heat flux model (EAHM) is introduced as a function of the strain rate and vorticity tensor with the Cayley–Hamilton theorem (Pope, 1975). To secure an accurate near-wall behavior, a formulation of the thermal damping function f_λ is implemented with the wall damping function f_w. The model performance is demonstrated through comparisons with the data from several well-documented flows.

2. k–ε–f_μ model

2.1. Governing equations

For an incompressible turbulent flow, the governing equations can be written in Cartesian tensor notation as

$$\frac{\partial U_i}{\partial x_i} = 0, \tag{1}$$

$$U_j\frac{\partial U_i}{\partial x_j} = -\frac{1}{\rho}\frac{\partial P}{\partial x_i} + \frac{\partial}{\partial x_j}\left[\nu\frac{\partial U_i}{\partial x_j} - \overline{u_iu_j}\right], \tag{2}$$

where U_j and u_j are the jth components of the mean and fluctuating velocities, respectively. P is the mean pressure, ρ and ν are the fluid density and kinematic viscosity. In the k–ε–f_μ model of Park and Sung (1997), the unknown Reynolds stress $-\overline{u_iu_j}$ can be expressed in a conventional form as

$$-\overline{u_iu_j} = \nu_t\left(\frac{\partial U_i}{\partial x_j} + \frac{\partial U_j}{\partial x_i}\right) - \frac{2}{3}k\delta_{ij} - \tau_{ij}^N, \tag{3}$$

$$\nu_t = C_\mu f_\mu\frac{k^2}{\varepsilon}, \tag{4}$$

$$U_j\frac{\partial k}{\partial x_j} = \frac{\partial}{\partial x_j}\left[\left(\nu + \frac{\nu_t}{\sigma_k}\right)\frac{\partial k}{\partial x_j}\right] + P_k - \varepsilon, \tag{5}$$

$$U_j\frac{\partial\varepsilon}{\partial x_j}=\frac{\partial}{\partial x_j}\left[\left(\nu+\frac{\nu_t}{\sigma_\varepsilon}\right)\frac{\partial\varepsilon}{\partial x_j}\right]+\left(C^*_{\varepsilon1}P_k-C_{\varepsilon2}f_2\varepsilon\right)/T+C_{\varepsilon3}(1-f_w)\nu\nu_t\left(\frac{\partial^2U_i}{\partial x_j\partial x_k}\right)^2. \tag{6}$$

In the above, the tensor τ^N_{ij} represents the nonlinear part of Reynolds stresses: $\tau^N_{ij}=\tau^{\text{quadratic}}_{ij}-\tau^{\text{linear}}_{ij}$ or $\tau^N_{ij}=\tau^{\text{cubic}}_{ij}-\tau^{\text{linear}}_{ij}$. The production of turbulent kinetic energy P_k is defined as $P_k\equiv-\overline{u_iu_j}\partial U_i/\partial x_j$. The model function f_2 is expressed as $f_2=1-(2/9)\exp(-0.33R_t^{1/2})$, which describes the effect of decaying turbulence (Coleman and Mansour, 1992). The turbulent timescale is defined as $T=((k/\varepsilon)^2+36T_K^2)^{1/2}$ (Durbin and Laurence, 1996). The model constants are set as $C_\mu=0.09$, $\sigma_k=1.1$, $\sigma_\varepsilon=1.3$, $C_{\varepsilon2}=1.9$ and $C_{\varepsilon3}=0.8$, respectively. The variations of the eddy viscosity are allowed by decomposing f_μ into two parts, i.e., $f_\mu=f_{\mu1}f_{\mu2}$, where $f_{\mu1}$ signifies the effect of wall-proximity in the near-wall region while $f_{\mu2}$ represents the effect of nonequilibrium away from the wall (Park and Sung, 1995). The damping function $f_{\mu1}$ is obtained by solving a Helmholtz-type elliptic f_w equation.

$$f_{\mu1}=\left(1+f_DR_t^{-3/4}\right)f_w^2, \tag{7}$$

$$\frac{\partial^2f_w}{\partial x_j\partial x_j}=\frac{R_t^{3/2}}{A^2L^2}(f_w-1). \tag{8}$$

Here, the f_D function is defined as $f_D=10\times\exp[-(R_t/120)^2]$ and L is a turbulence length scale $L=k^{1.5}/\varepsilon$. As close to the wall, L becomes singular. In order to regularize the length scale, the Kolmogorov scale is adopted as a lower bound $L^2=k^3/\varepsilon^2+70^2\sqrt{\nu^3/\varepsilon}$ (Durbin and Laurence, 1996). Details regarding the model derivation can be found in Park and Sung (1997). Note that L is slightly modified from the original version of Park and Sung (1997) to simplify the model constant ($A=8.4$).

The derivation of $f_{\mu2}$ is originated from the Reynolds stress transport equation in a homogeneous flow with a local equilibrium state. A general algebraic form of the anisotropy tensor $b_{ij}=\overline{u_iu_j}/2k-\delta_{ij}/3$ is obtained by employing the model of Speziale et al. (1991),

$$b_{ij}2g=\left(C_2-\frac{4}{3}\right)S^*_{ij}+(C_3-2)\left(b_{ik}S^*_{jk}+b_{jk}S^*_{ik}-\frac{2}{3}b_{mn}S_{mn}\delta_{ij}\right)+(C_4-2)\left(b_{ik}W^*_{jk}+b_{jk}W^*_{ik}\right), \tag{9}$$

where $S^*_{ij}=S_{ij}k/\varepsilon$, $W^*_{ij}=W_{ij}k/\varepsilon$ and $g=C_1/2+P_k/\varepsilon-1$, respectively. The model constants C_1–C_4 are employed from the evaluation of Gatski and Speziale (1993), i.e., $C_1=6.8$, $C_2=0.36$, $C_3=1.25$ and $C_4=0.4$. In a matrix form, Eq. (9) can be written as

$$\mathbf{b}=\alpha_1\mathbf{S}+\alpha_2\left(\mathbf{bS}+\mathbf{Sb}-\frac{2}{3}\{\mathbf{bS}\}\mathbf{I}\right)+\alpha_3(\mathbf{Wb}-\mathbf{bW}), \tag{10}$$

where the model constants are summarized as $\alpha_1=(C_2-4/3)/2g$, $\alpha_2=(C_3-2)/2g$ and $\alpha_3=(C_4-2)/2g$. $\{.\}$ Denotes the trace and $\mathbf{I}$ is the identity vector. For a two-dimensional flow, an explicit expression of $\mathbf{b}$ is available in linearly-independent tensors that may be formed with $\mathbf{S}$ and $\mathbf{W}$ (Gatski and Speziale, 1993). The third-order form of algebraic solution is

$$\mathbf{b}=\beta_1\mathbf{S}+\beta_2\left(\mathbf{S}^2-\frac{1}{3}\{\mathbf{S}^2\}\mathbf{I}\right)+\beta_3(\mathbf{SW}-\mathbf{WS})+\beta_4\left(\mathbf{S}^2\mathbf{W}-\mathbf{WS}^2\right)+\beta_5\left(\mathbf{W}^2\mathbf{S}+\mathbf{SW}^2-\{\mathbf{W}^2\}\mathbf{IS}-\frac{2}{3}\{\mathbf{WSW}\}\mathbf{I}\right). \tag{11}$$

To determine the coefficients β_1–β_5, the substitution of Eq. (11) into Eq. (10) gives a nonlinear stress–strain relation. All higher-order tensor combinations are reduced with the aid of the Cayley–Hamilton theorem (Pope, 1975)

$$\mathbf{b}=\alpha_1\mathbf{S}+\frac{1}{3}\alpha_2\beta_2\{\mathbf{S}^2\}\mathbf{S}+2\alpha_3\beta_3\{\mathbf{W}^2\}\mathbf{S}+2\alpha_2\beta_1\left(\mathbf{S}^2-\frac{1}{3}\{\mathbf{S}^2\}\mathbf{I}\right)+\alpha_3\beta_1(\mathbf{WS}-\mathbf{SW})+(\alpha_3\beta_2-\alpha_2\beta_3)\left(\mathbf{WS}^2-\mathbf{S}^2\mathbf{W}\right)-\alpha_3\beta_3\left(\mathbf{W}^2\mathbf{S}+\mathbf{SW}^2-\{\mathbf{W}^2\}\mathbf{IS}-\frac{2}{3}\{\mathbf{WSW}\}\mathbf{I}\right). \tag{12}$$

The model coefficients are determined by comparing it with Eq. (11).

$$\beta_1=\frac{\alpha_1}{1-\frac{2}{3}\alpha_2^2S^*_{mn}S^*_{mn}+2\alpha_3^2W^*_{mn}W^*_{mn}},\quad \beta_2=2\alpha_2\beta_1$$
$$\beta_3=-\alpha_3\beta_1,\quad \beta_4=\alpha_2\beta_3-\alpha_3\beta_2,\quad \beta_5=-\alpha_3\beta_3. \tag{13}$$

This constitutes an anisotropic eddy-viscosity model with the strain-dependent coefficients. As expressed previously, the coefficients $\alpha_1-\alpha_3$ are dependent on $g=C_1/2+P_k/\varepsilon-1$. It is possible to obtain an explicit solution with a fixed value of g (Gatski and Speziale, 1993). However, g varies depending on the flow condition. The variation of g needs to be accounted for the nonlinear stress–strain relation.

In general, P_k/ε is expressed as $P_k/\varepsilon=-2\{\mathbf{bS}\}=2\beta_1S^*_{mn}S^*_{mn}$. From Eq. (13), we get the following relation:

$$\beta_1=\frac{C_0-g}{\eta^2}=\frac{\tilde\alpha_1 g}{g^2+A_s} \tag{14}$$

$$g^3-C_0g^2+(A_s+\tilde\alpha_1\eta^2)g-C_0A_s=0, \tag{15}$$

where $A_s=\tilde\alpha_3^2\xi^2-\tilde\alpha_2^2\eta^2/3$ and $C_0=C_1/2-1$. Here, the model constants are $\tilde\alpha_1=\alpha_1g$, $\tilde\alpha_2=\alpha_2g$ and $\tilde\alpha_3=\alpha_3g$.

The mean strain rates are defined by $S^* = \sqrt{2S^*_{ij}S^*_{ij}}$, $W^* = \sqrt{2W^*_{ij}W^*_{ij}}$, $\eta = f_w S^*$ and $\xi = f_w W^*$. The introduction of f_w in the variables η and ξ is placed on the fact that the wall-proximity effect in the vicinity of the wall is significant compared to the strain rate effect.

The above Eq. (15) can be solved in the following. For a general case, Girimaji (1996) showed that the cubic equation can produce multiple real roots. A proper choice is needed among the possible roots. However, Wallin and Johansson (2000) proposed a simple procedure similar to that of Girimaji (1996), which is applied to Eq. (15). The final solution is obtained as

$$g = \begin{cases} \dfrac{C_0}{3} + (P_1 + \sqrt{P_2})^{1/3} + \mathrm{sign}(P_1 - \sqrt{P_2})|P_1 - \sqrt{P_2}|^{1/3}, \\ \quad P_2 \geqslant 0, \\ \dfrac{C_0}{3} + 2(P_1^2 - P_2)^{1/6} \cos\left(\dfrac{1}{3}\arccos\left(\dfrac{P_1}{\sqrt{P_1^2 - P_2}}\right)\right), \\ \quad P_2 < 0. \end{cases} \tag{16}$$

Here, P_1 and P_2 are defined as

$$P_1 = C_0\left[\frac{C_0^2}{27} - \frac{(A_s + \tilde{\alpha}_1\eta^2)}{6} + \frac{1}{2}\right],$$
$$P_2 = P_1^2 - \left[\frac{C_0^2}{9} - \frac{(A_s + \tilde{\alpha}_1\eta^2)}{3}\right]. \tag{17}$$

Note that the variable g is real and positive for all possible values of S^* and W^*.

From the linear term in Eq. (11), the damping function $f_{\mu 2}$ has the relation as $f_{\mu 2} = -\beta_1/C_\mu$. However, the coefficient β_1 in Eq. (13) is not realizable for an irrotational flow, i.e., $W^* = 0$. This gives an excessive turbulence production in an impinging jet flow. Accordingly, the damping function $f_{\mu 2}$ is modified as $f_{\mu 2} = (15/3)(1+g)/(g^2 + C_\mu g^3 + A_s)$. The model constants are determined from the model of Speziale et al. (1991): $C_0 = 2.4$, $\tilde{\alpha}_1 = -0.48$, $\tilde{\alpha}_2 = -0.375$ and $\tilde{\alpha}_3 = -0.8$. To check the model performance, the behaviors of $C_\mu f_{\mu 2}$ are plotted in Fig. 1. The value of $C_\mu f_{\mu 2}$ can be obtained from the relation of P_k/ε, i.e., $C_\mu f_{\mu 2} = P_k/(\varepsilon S^{*2})$ and $C_\mu f_{\mu 2} = -2b_{12}/S^*$. The predicted results are compared with the DNS data (Lee et al., 1990) and for $P_k/\varepsilon = (C_{\varepsilon 2} - 1)/(C^*_{\varepsilon 1} - 1) \sim 1.89$ and $P_k/\varepsilon = 1$. The model of Gatski and Speziale (1993) is adopted for comparison. For a homogeneous shear flow, the present model prediction is in good agreement with the DNS data. For an irrotational flow ($W^* = 0$), it is seen that the model of Gatski and Speziale (1993) departs significantly from the general behavior, i.e., $C_\mu f_{\mu 2}$ decreases with increasing S^*. This violates the realizability condition for $W^* = 0$ (Park and Sung, 2001). However, the present model shows a similar behavior to that of a homogeneous shear flow.

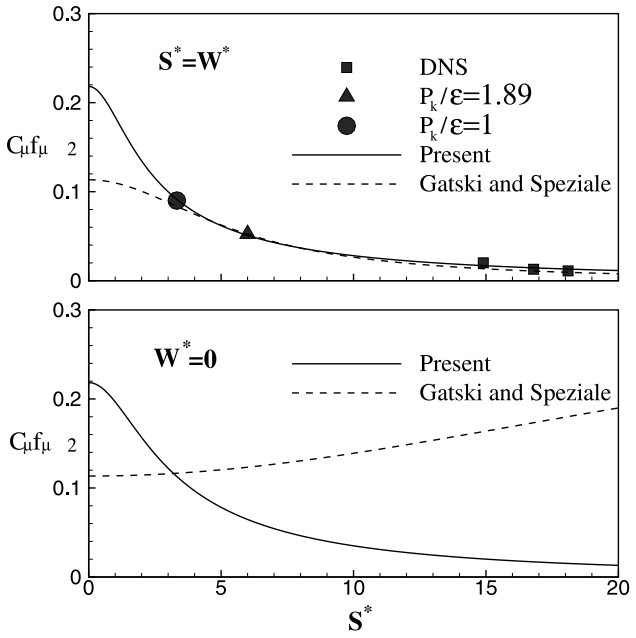

Fig. 1. Behaviors of $C_\mu f_{\mu 2}$ for a simple shear flow.

In general, a constant value of $C^*_{\varepsilon 1}$ is employed in many k–ε models. It is well known that the variation of $C^*_{\varepsilon 1}$ gives a significant influence on the reattachment length prediction in flows over a backward-facing step (Park and Sung, 1997). This may be attributed to the additional production of the dissipation rate by local anisotropy. In order to incorporate the effect of rotational strains, a new $C^*_{\varepsilon 1}$ is devised as $C^*_{\varepsilon 1} \sim 1 + (C_{\varepsilon 2} - 1)/(P_k/\varepsilon)_\infty$ (Speziale and Gatski, 1997). Based on $P_k/\varepsilon \sim C_\mu f_{\mu 2} S^{*^2}$, $C^*_{\varepsilon 1}$ is modeled as $C^*_{\varepsilon 1} = 1.42 + C_\mu/(1 + 5f_{\mu 2}\eta^2)$.

3. Stress–strain relation

Many versions of the EASM have been developed on the basis of homogeneous turbulent flows in a equilibrium state (Apsley and Leschziner, 1998; Craft et al., 1996; Gatski and Speziale, 1993; Girimaji, 1996; Wallin and Johansson, 2000). This strategy retains the major physical behavior from the second-order closure and keeps the robustness of linear eddy-viscosity models. In the previous section, we derived a third-order nonlinear τ_{ij} in Eq. (11). The nonlinear extension of the 'linear' τ_{ij} can be summarized as

$$\tau_{ij}^{\mathrm{linear}} = \tfrac{2}{3}k\delta_{ij} - 2kC_\mu f_\mu S^*_{ij}, \tag{18}$$

$$\tau_{ij}^{\mathrm{quadratic}} = \tau_{ij}^{\mathrm{linear}} + k(\tilde{\beta}_2 + \tilde{\beta}_{2,\mathrm{wall}}C_w)\left(S^*_{ik}S^*_{kj} - \frac{1}{3}S^{*^2}\delta_{ij}\right) \tag{19}$$

$$+ k(\tilde{\beta}_3 + \tilde{\beta}_{3,\mathrm{wall}}C_w)\left(W^*_{ik}S^*_{kj} - S^*_{ik}W^*_{kj}\right), \tag{20}$$

$$\tau_{ij}^{\text{cubic}} = \tau_{ij}^{\text{quadratic}} + k\tilde{\beta}_4\left(S_{il}^*S_{lm}^*W_{mj}^* - W_{il}^*S_{lm}^*S_{mj}^*\right) + k\tilde{\beta}_5\left(W_{il}^*W_{lm}^*S_{mj}^* + S_{il}^*W_{lm}^*W_{mj}^* + 0.5S_{ij}^*W^{*^2} - \frac{2}{3}III_S\delta_{ij}\right), \tag{21}$$

where $\tilde{\beta}_i$ are the model coefficients pertaining to Eq. (13) and $III_S = S_{lm}^*W_{mn}^*W_{nl}^*$. The wall corrections of the present $\tilde{\beta}_i$ is restricted to the normal Reynolds stresses because the linear model gives a good prediction of Reynolds shear stresses, i.e., $C_w = 1$ for $i = j$ and $C_w = 0$ for $i \neq j$. Away from the wall, the parent model of the present derivation gives the values of $\tilde{\beta}_i$. However, since the wall effect is not included in the pressure–strain correlation, the model is not available in wall-bounded flows.

To calibrate the model constants, the realizability constraint is imposed on $\tilde{\beta}_i$. Here, the near-wall treatment is excluded ($f_w = 1$, $\tilde{\beta}_{2,\text{wall}} = \tilde{\beta}_{3,\text{wall}} = 0$). For example, in a simple shear flow, the Reynolds stress tensor has the form as

$$\begin{aligned}
\overline{u_1^2}/k &= \frac{2}{3} + \tilde{\beta}_2\frac{S^{*^2}}{12} + \tilde{\beta}_3\frac{S^*W^*}{2},\\
\overline{u_2^2}/k &= \frac{2}{3} + \tilde{\beta}_2\frac{S^{*^2}}{12} - \tilde{\beta}_3\frac{S^*W^*}{2},\\
\overline{u_3^2}/k &= \frac{2}{3} - \tilde{\beta}_2\frac{S^{*^2}}{6},\\
\overline{u_1u_2}/k &= -C_\mu f_{\mu 2}S^*,
\end{aligned} \tag{22}$$

where $S_{12}^* = S_{21}^* = 0.5S^*$, $W_{12}^* = -W_{21}^* = 0.5W^*$ and other terms $= 0$. The nonnegative condition gives the realizable range as $0 \leqslant \tilde{\beta}_2 \leqslant 4/(S^*)^2$. The Schwarz' inequality yields $\tilde{\beta}_3(S^*W^*/2) \leqslant (B^2 - (C_\mu f_{\mu 2}S^*)^2)^{1/2}$ and $B = 2/3 + \tilde{\beta}_2 S^{*^2}/12$. Considering the above realizability conditions, the following relation is obtained: $0 \leqslant \tilde{\beta}_2 \leqslant 4/(S^*)^2$ and $0 \leqslant f_{\mu 2} \leqslant 2/(3C_\mu S^*)$. The realizable range of $\tilde{\beta}_3$ is $0 \leqslant \tilde{\beta}_3 \leqslant (1 - (C_\mu f_{\mu 2}S^*)^2)^{1/2}/(S^*W^*/2)$. These provide the realizability limits of $\tilde{\beta}_i$ without the wall corrections.

In a simple shear flow, the near-wall behavior of the normal Reynolds stress is controlled by $\tilde{\beta}_{2,\text{wall}}$ and $\tilde{\beta}_{3,\text{wall}}$. From the DNS data (Moser et al., 1999), the limiting values of b_{11} and b_{22} are $b_{11} = B_1 - 1/3$ and $b_{22} = -1/3$ as $y \to 0$. Here, B_1 is a constant. These limiting values are not obtained by $\tilde{\beta}_i$ in Eq. (13), because there are no wall reflection and viscous effects. To obtain the correct behavior in the near-wall region, $\tilde{\beta}_i$ should be modified in a way similar to the low Reynolds number models (Apsley and Leschziner, 1998). The f_w function is used as a blending of the near-wall corrections with the outer-region anisotropies. The modeled coefficients are obtained as

$$\tilde{\beta}_2 = C_\mu f_{S1}f_w^2, \quad \tilde{\beta}_3 = C_\mu f_{S2}f_w^2,$$

$$\tilde{\beta}_{2,\text{wall}} = (1 - f_w)2.5S_B/S_w,$$

$$\tilde{\beta}_{3,\text{wall}} = (1 - f_w)(1.8S_B/S_w - \tilde{\beta}_3),$$

$$\tilde{\beta}_4 = -C_\mu(f_{S1}f_w)^2, \quad \tilde{\beta}_5 = C_\mu(f_{S2}f_w)^2,$$

where $f_{S1} = (1 + \eta_s f_{\mu 2})/(1 + 4\eta_s + 4\eta_s^2)$, $f_{S2} = (1 + \eta_s f_{\mu 2})/(1 + \eta_s + 8\eta_s^2)$ and $\eta_s = C_\mu\text{MAX}(\eta, \xi)$. To correct the wall behaviors ($y^+ \leqslant 100$), the modified strain variable S_w is introduced. In the vicinity of the wall, S_w has to maintain the relation $S_w \sim O(S^{*^2})$. This is because the limiting values of b_{11} and b_{22} have a nonzero value. Based on the above behavior, a modified strain variable S_w is modeled as $S_w = 1 + [\text{MAX}(S^*, W^*)]^2$. In order to avoid a negative stress, the parameter S_B is introduced as $S_B = 2S_{mn}S_{mn}(1 - \delta_{mn})/S^{*^2}$. This ensures the realizable normal stresses in the near-wall region deviated from a simple shear flow.

To check the realizability of $\tilde{\beta}_i$, the behaviors of $\tilde{\beta}_2$ and $\tilde{\beta}_3$ without the wall corrections ($\tilde{\beta}_{2,\text{wall}} = \tilde{\beta}_{3,\text{wall}} = 0$) are examined for a simple shear flow ($W^* = S^*$). As can be seen in Fig. 2, the modeled coefficients lie within the realizability limitation. Note that the functional forms of $\tilde{\beta}_i$ have been tuned in a homogeneous flow ($f_w = 1$). The model validation is checked by showing the anisotropy prediction by the present model coefficients. The model of Craft et al. (1996) is also adopted for comparison. As shown in Fig. 3, the normal stress

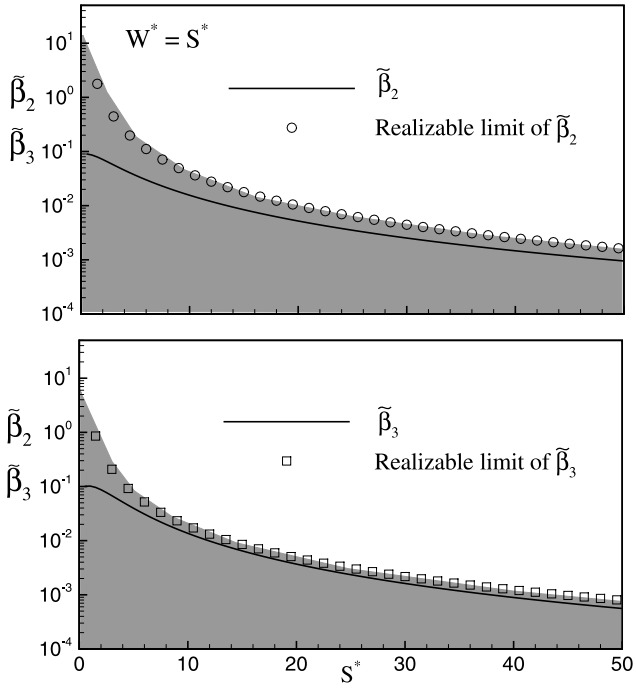

Fig. 2. Behaviors of $\tilde{\beta}_2$, $\tilde{\beta}_3$ in the realizable range: $0 \leqslant \tilde{\beta}_2 \leqslant 4/(S^*)^2$ and $0 \leqslant \tilde{\beta}_3 \leqslant (1 - (C_\mu f_{\mu 2}S^*)^2)^{1/2}/(S^*W^*/2)$.

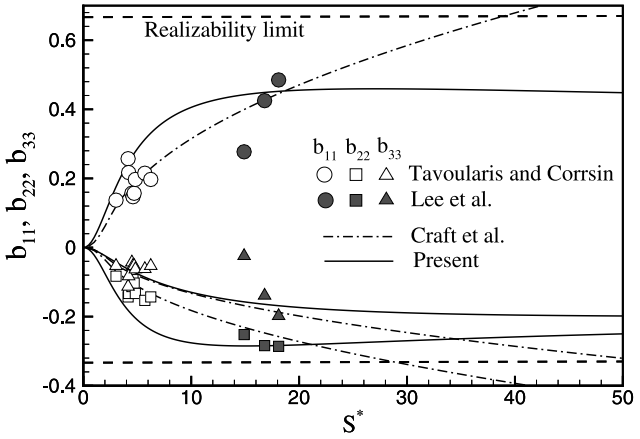

Fig. 3. Predictions of b_{11}, b_{22} and b_{33} by turbulence models.

anisotropies are in good agreement with the experimental (Tavoularis and Corrsin, 1981) and DNS data (Lee et al., 1990). The model prediction of Craft et al. (1996) shows an increasing behavior in highly strained regions ($S^* \geqslant 30$). This is attributed to the fact that the quadratic terms of their nonlinear model increase with increasing $\sqrt{S^*}$. As expected, the present model satisfies the realizability limitation well. To look into the roles of $\tilde{\beta}_{2,\mathrm{wall}}$ and $\tilde{\beta}_{3,\mathrm{wall}}$ for a fully developed channel flow, the near-wall behaviors of Reynolds stresses are displayed in Fig. 4. The near-wall anisotropies are strongly affected by $\tilde{\beta}_{2,\mathrm{wall}}$ and $\tilde{\beta}_{3,wall}$ in the region of $y^+ \leqslant 100$. The present model is fully realizable and reproduces the nonlinear relation well in the near-wall region. However, the wall correction has a minor effect in the range of $y^+ \leqslant 5$.

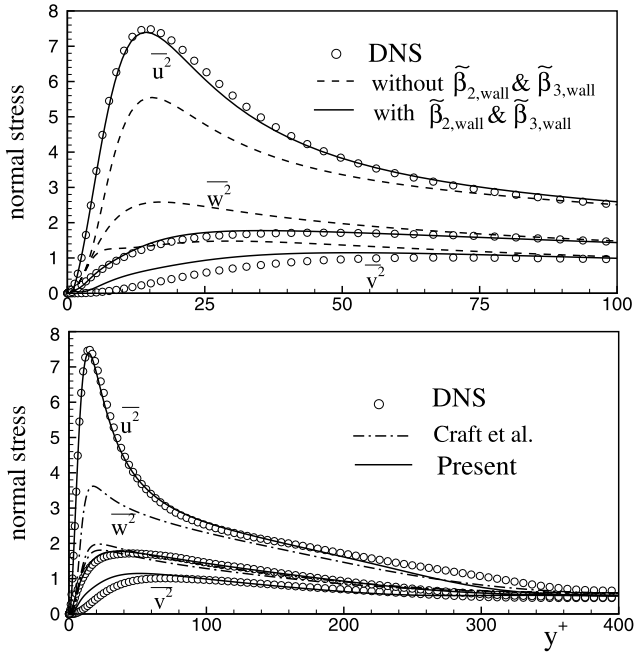

Fig. 4. Comparison of $\overline{u^2}^+$, $\overline{v^2}^+$ and $\overline{w^2}^+$ with DNS (Moser et al., 1999).

4. Explicit algebraic heat flux model

The governing equation of mean temperature can be expressed as

$$U_j \frac{\partial T}{\partial x_j} = \frac{\partial}{\partial x_j}\left[\frac{\nu}{Pr}\frac{\partial T}{\partial x_j} - \overline{\theta u_j}\right]. \tag{23}$$

In a manner similar to the derivation of velocity model, a nonlinear heat flux model is obtained by employing the strain-dependent functions. An algebraic heat flux model satisfies the relation, $\overline{\theta u_i}(\varepsilon/k) = -\overline{u_i u_j} T_{,j} - \overline{\theta u_j}\partial U_i/\partial x_j$ (Abe et al., 1996; Rogers et al., 1989; So and Sommer, 1996). This is rewritten by the following notation:

$$b_{\theta i} = -\left(\frac{2}{3}\delta_{ij} + 2b_{ij}\right)T^*_{,j} - \left(S^\theta_{ij} + W^\theta_{ij}\right)b_{\theta j}, \tag{24}$$

where $b_{\theta i} = \overline{\theta u_i}/\sqrt{k}T_{\mathrm{ref}}$, $S^\theta_{ij} = C_{T2}S_{ij}(k/\varepsilon)$, $W^\theta_{ij} = C_{T3}W_{ij}(k/\varepsilon)$ and $T^*_{,j} = C_{T1}T_{,j}(k^{1.5}/\varepsilon T_{\mathrm{ref}})$. Here, $C_{T1} = 1/C_{1\theta}$, $C_{T2} = (1 - C_{2\theta} - C_{3\theta})/C_{1\theta}$ and $C_{T3} = (1 - C_{2\theta} + C_{3\theta})/C_{1\theta}$ and $C_{1\theta} \sim C_{3\theta}$ are model constants (Launder, 1988).

From the above equations, the heat flux is expressed implicitly. To solve the heat flux, an EAHM is derived in the present study for strongly strained flow. Recently, to avoid the implicit relation, several models have been proposed (Abe et al., 1996; Rhee and Sung, 2000; Rogers et al., 1989; Shabany and Durbin, 1997; So and Sommer, 1996). In the present study, the quadratic relation of the strain rate and vorticity tensor is developed to consider the nonlinear heat transfer. Let us assume $\overline{\theta u_i} = f(\overline{u_i u_j}, S_{ij}, W_{ij}, T_{,i}, k, \varepsilon)$. Under the assumption, a matrix form of the explicit solution is obtained,

$$\begin{aligned}\mathbf{b}^* = &\left[\gamma_1\left(\frac{2}{3}\mathbf{I} + 2\mathbf{b}\right) + \gamma_2(\mathbf{S} + \mathbf{W})\right]\mathbf{T} \\ &+ \left[\gamma_3(\mathbf{S}^2 + \mathbf{W}^2) + \gamma_4(\mathbf{SW} + \mathbf{WS})\right]\mathbf{T}.\end{aligned} \tag{25}$$

From the substitution of Eq. (25) into Eq. (24), we derive an explicit expression which provides a canonical form of the nonlinear heat flux. The Cayley–Hamilton theorem (Pope, 1975) is applied to the higher-order terms,

$$\begin{aligned}&\mathbf{S}^3 = (1/3)\{\mathbf{S}^3\}\mathbf{I} + (1/2)\{\mathbf{S}^2\}\mathbf{IS}, \\ &\mathbf{SW}^2 + \mathbf{WS}^2 = (1/2)\{\mathbf{W}^2\}\mathbf{IS} + (1/2)\{\mathbf{S}^2\}\mathbf{IW}, \\ &\mathbf{W}^3 = (1/3)\{\mathbf{W}^3\}\mathbf{I} + (1/2)\{\mathbf{W}^2\}\mathbf{IW}, \\ &\mathbf{S}^2\mathbf{W} + \mathbf{SWS} + \mathbf{WSW} + \mathbf{W}^2\mathbf{S} = 0.\end{aligned} \tag{26}$$

Then, the final coefficients are obtained as

$$\begin{aligned}&\gamma_1 = -1, \quad \gamma_3 = -\gamma_2, \quad \gamma_4 = -\gamma_2, \\ &\gamma_2\mathbf{I} = (2\mathbf{I}/3 + 2\mathbf{b})/[\mathbf{I} - 0.5(\{\mathbf{S}^2\} + \{\mathbf{W}^2\})].\end{aligned} \tag{27}$$

It is interesting to find that γ_2 arrives at the same form as that of Abe et al. (1996). In the deviated condition from a simple shear flow ($S^\theta_{ij}S^\theta_{ij}/C^2_{T2} \neq W^\theta_{ij}W^\theta_{ij}/C^2_{T3}$), the coefficient γ_2 is only affected by the deformation variable

$\eta_t^* = \xi_t^2 - \eta_t^2$, where $\eta_t = (S_{ij}^\theta S_{ij}^\theta)^{1/2}$ and $\xi_t = (W_{ij}^\theta W_{ij}^\theta)^{1/2}$. The strain dependent variable $\gamma_2 = 1/(1+0.5\eta_t^*)$ is singular at $\eta_t^* = -2$. It is found that $\gamma_2 \to 1$ for $\eta_t^* \to 0$ and $\gamma_2 \to 0$ for $\eta_t^* \to \infty$. Based on the regularization procedure developed by Gatski and Speziale (1993), the γ_2 function can be expressed as $\gamma_2 = (1+\eta_t^*)/(1+1.5\eta_t^*)$. However, it is also singular at $\eta_t^* = -2/3$. The γ_2 function is simply rewritten by $\gamma_2 \sim (2+\eta_t^*)/(2+\eta_t^* + 0.5\eta_t^*(2+\eta_t^*))$. This equation is modeled as $\gamma_2 \sim (2+\eta_t^*)/(2+\xi_s^2 + \eta_t^*(1+\eta_t^*))$ with $\xi_s = \mathrm{MAX}(\xi_t^2, \eta_t^2)$. In strongly strained flows, γ_2 prevents an excessive increase of the strain dependent terms. From the experiment of Tavoularis and Corrsin (1981), the model constants C_{T2} and C_{T3} are optimized as $C_{T2} = 0.2$ and $C_{T3} = 0.12$. The present model gives the heat-flux ratio $\overline{u\theta}/\overline{v\theta} = -6.3$ at $T_{,1} \neq 0$ and $\overline{u\theta}/\overline{v\theta} = -1.75$ at $T_{,2} \neq 0$. To see the strain effects, three variations of $\overline{\theta u_i}$ are examined in the present study on the basis of Eq. (25). The final explicit heat flux models are summarized as

$$\overline{\theta u_i}^{\text{zeroth}} = -\alpha_t \left(\frac{2}{3}\delta_{ij} + 2 f_w b_{ij} \right) T_{,j}, \tag{28}$$

$$\overline{\theta u_i}^{\text{first}} = \overline{\theta u_i}^{\text{zeroth}} - \alpha_{ik}\left(S_{km}^\theta + W_{km}^\theta\right) T_{,m}, \tag{29}$$

$$\overline{\theta u_i}^{\text{second}} = \overline{\theta u_i}^{\text{first}} - 2\alpha_{ik}\left(S_{kl}^\theta S_{lm}^\theta + W_{kl}^\theta W_{lm}^\theta + S_{kl}^\theta W_{lm}^\theta + W_{kl}^\theta S_{lm}^\theta\right) T_{,m}, \tag{30}$$

$$\gamma_2 = \frac{f_w(2+\eta_t^*)}{2+\xi_s^2+\eta_t^*(1+\eta_t^*)}, \tag{31}$$

where $\alpha_{ik} = \alpha_t \gamma_2 (\overline{u_i u_k}/k)$. When compared with the preceding models, the present model includes the quadratic effects of flow deformation. As addressed in Rhee and Sung (2000), the nonlinear terms play a dominant role in predicting the convective heat transfer of complex separated and reattaching flows. Eq. (25) is similar to their model, however, their nonlinear terms may give rise to unrealizable solutions in strongly strained flows. It is seen that the present γ_2 has a regular solution depending on the flow condition. The introduction of f_w ensures that $\overline{\theta u_i}^{\text{zeroth}}$ is dominant in the near-wall region.

Based on the proposal of Rogers et al. (1989), the thermal diffusivity is expressed as $\alpha_t = C_\lambda f_\lambda \nu_t$. The coefficient C_λ is a function of R_t and Pr. The near-wall effect of α_t is incorporated in the f_λ function. It is known that the near-wall asymptotic behavior is derived as $-\overline{v\theta} \sim y^3$ and $\partial T/\partial y \sim y^0$. To satisfy the asymptotic behavior, the coefficient C_λ and the f_λ function are modeled as

$$f_\lambda = [1 - \exp(-8 f_w)]^3, \tag{32}$$

$$C_\lambda = \frac{2}{3}\left(1 + \frac{12.5}{R_t^{0.5}}\right)^2 \left(1 + \frac{130}{R_t Pr}\right)^{-0.25}. \tag{33}$$

This model satisfies the asymptotic near-wall behavior, $-\overline{v\theta} \sim y^3$.

5. Results and discussion

Before proceeding further, it is important to ascertain the reliability and accuracy of the present model. Toward this end, we have applied the model to a fully developed channel flow, for which turbulence quantities are available from the DNS data (Moser et al., 1999). Next, the nonlinear effects of the present model are tested in separated and reattaching flows and strongly strained impinging jet flows.

5.1. Numerical procedure

The governing equations were discretized using the hybrid linear and parabolic approximation scheme with second-order accuracy. A nonstaggered variable arrangement was adopted with the momentum interpolation technique to avoid the pressure–velocity decoupling. The coupling between pressure and velocity was achieved by the SIMPLEC algorithm. The grid dependency was checked and the solution was accelerated with a multigrid method (Park, 1999). Convergence was declared when the maximum normalized sum of absolute residual source over all the computational nodes was less than 10^{-4}. Details regarding the numerical procedure are compiled in Park and Sung (1997).

5.2. Channel flow

The selected Reynolds number is $Re_\tau = 395$. The profiles of mean velocity, turbulent kinetic energy, its dissipation rate and Reynolds stress are displayed in Fig. 5. For a fully developed channel flow, the stress–strain relation becomes the linear relation, because the streamwise gradients are free. The results of the present model are in good agreement with the DNS data (Moser et al., 1999). Fig. 6 shows the predicted mean temperature profile in a fully developed channel flow by using the present nonlinear heat flux model. A good agreement with the DNS data (Kasagi et al., 1992) is shown in the mean temperature prediction. However, the predicted data by using the constant Pr_t assumption is slightly underpredicted.

5.3. Backward-facing step flow

In order to look into the present model performance for separated and reattaching flows, two experimental data are employed for comparison (Driver and Seegmiller, 1985; Eaton and Johnston, 1980). The flow configuration over a backward-facing step is frequently used for benchmarking the performance of turbulence models for separated and reattaching flows. The result of Vogel and Eaton (1985) is also adopted to validate the thermal field. Fig. 7 shows the distributions of mean velocity U/U_o and Reynolds stress $\overline{u^2}/U_o^2$ in the

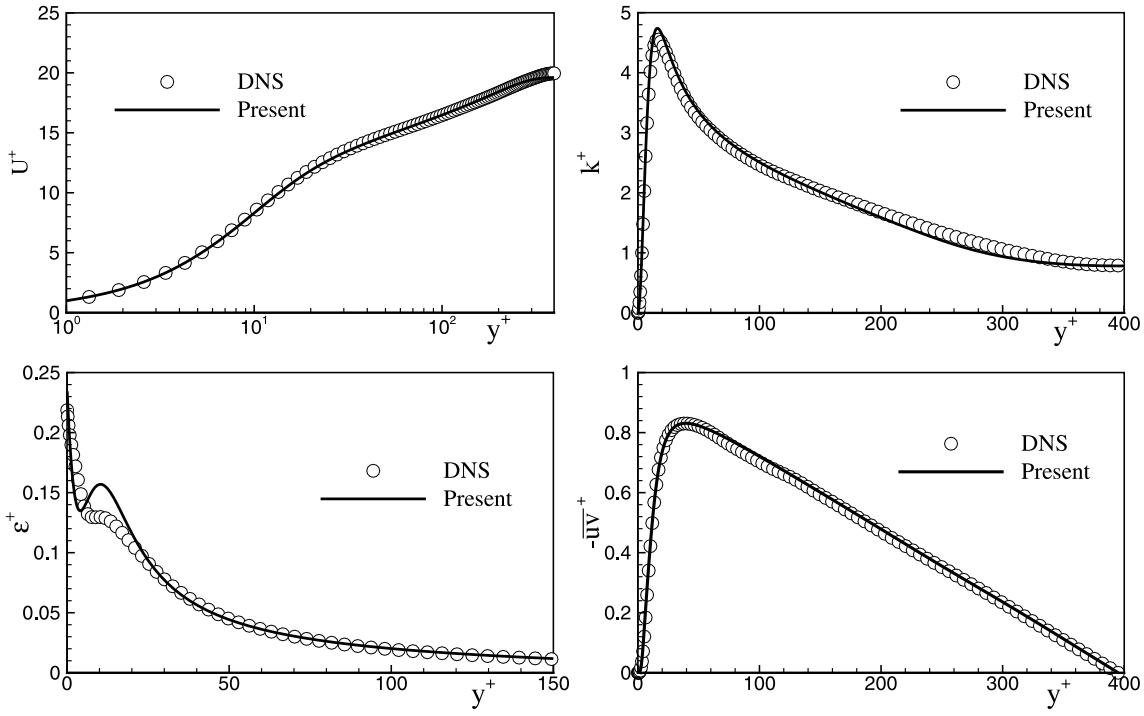

Fig. 5. Comparison of the predicted U^+, k^+, ε^+ and $-\overline{uv}^+$ with DNS (Moser et al., 1999).

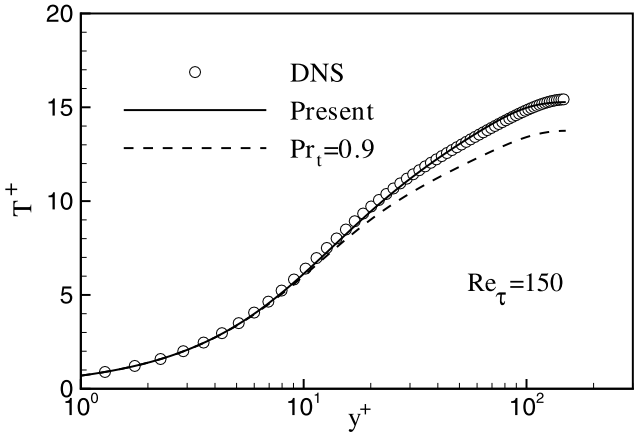

Fig. 6. Comparison of the predicted T^+ with DNS (Kasagi et al., 1992).

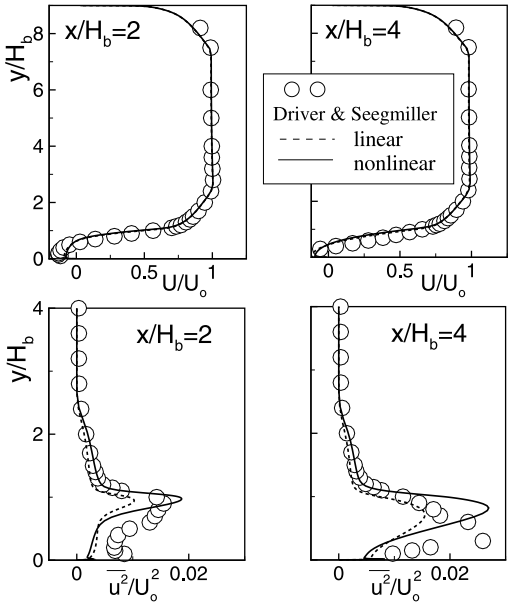

Fig. 7. Comparison of U/U_o and $\overline{u^2}/U_o^2$ with experiment.

recirculation region. The prediction of the nonlinear model is obtained by the present τ_{ij}^{cubic}. No big differences are shown between two model predictions for mean velocity. However, the linear model underpredicts the normal Reynolds stress, whereas the present nonlinear model predicts well. This appears to be a common feature that the linear stress–strain relation is insensitive to the nonlinear strain effects in the recirculating region.

Fig. 8 shows the distributions of the wall friction coefficient C_f downstream of the step. The top wall can be deflected to impose a pressure gradient on the recirculation region, where α is a top-wall deflection angle (Driver and Seegmiller, 1985). The prediction of C_f shows a good criterion of the model performance near the wall region for separated and reattaching flows. This is closely related to the near-wall characteristics of turbulence models. The linear model slightly overestimates C_f both in the recirculating region and in the recovery region, while the present nonlinear model shows an improved prediction. Compared with the linear model, the nonlinear model predicts a slightly longer reattach-

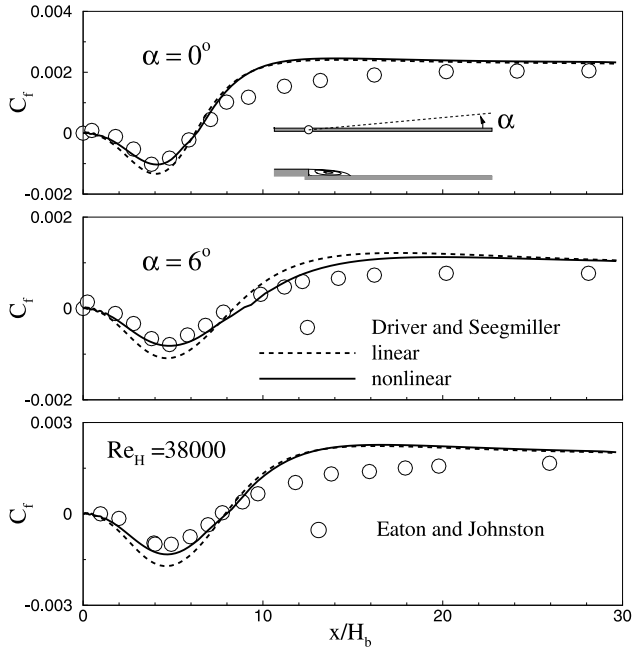

Fig. 8. Comparison of the predicted C_f with experiment.

ment length. The calculated reattachment lengths X_R/H_b are summarized in Table 1.

The stress–strain relation is examined with the present EAHM. To see the flow model influence on heat transfer, several model predictions for *St* are displayed in Fig. 9. The model performance of the present EAHM is validated by truncating the higher-order terms in the stress–strain relation. 'linear + EAHM' denotes that the standard form of $b_{ij} = -C_\mu f_\mu S^*_{ij}$ is employed ($\tau_{ij}^{\text{linear}} + \overline{\theta u_i}^{\text{second}}$). 'quadratic + EAHM' is that the nonlinear model is truncated to the quadratic term in the nonlinear model ($\tau_{ij}^{\text{quadratic}} + \overline{\theta u_i}^{\text{second}}$). When the cubic term is included, the model prediction is represented by 'cubic + EAHM'. As shown in Fig. 9, the overprediction by the linear model is clearly seen in the recirculation region. The quadratic model slightly overpredicts in the relaxing region after reattachment. However, the difference with the present cubic model is negligible. The nonlinear stress–strain relation gives a meaningful influence on the wall heat transfer rate.

Comparison is extended to the performance of the heat flux model, keeping the cubic stress–strain relation. Fig. 10 shows the predictions for various heat flux models. Before proceeding, the present heat flux model is tested with the conventional models. At first, the

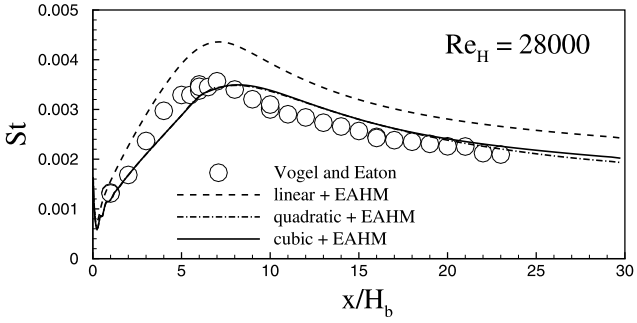

Fig. 9. Model comparisons of *St* with experiment.

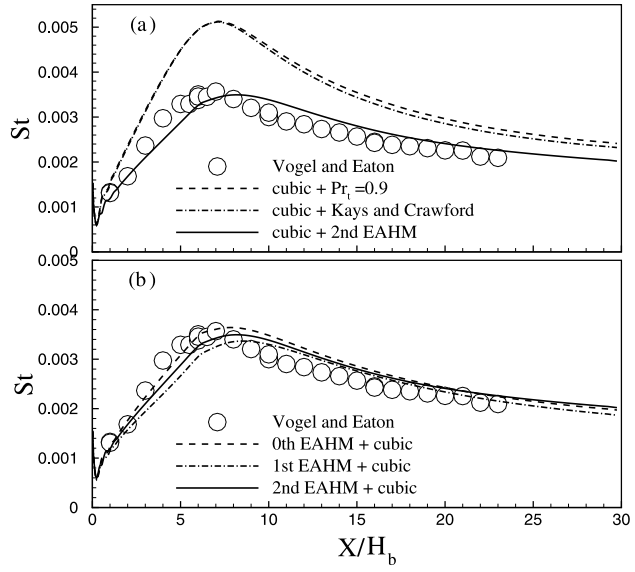

Fig. 10. Model comparisons of *St* with experiment.

constant Pr_t assumption is employed ($Pr_t = 0.9$). The well-known formula of Kays and Crawford (1993) is also adopted. The predicted results are displayed in Fig. 10(a), where the present EAHM predicts well with the experiment. It is seen that the assumption of constant Pr_t is no longer applicable to the strongly strained recirculation region. The formula of Kays and Crawford (1993) is also inappropriate for separated and reattaching flows. This is attributed to the weak variation of turbulent heat flux depending on the flow condition.

Finally, the strain effect of EAHM is examined keeping the cubic stress–strain relation. The 'nth' means the order of the strain rate according to Eqs. (28)–(30). The predicted results in Fig. 10(b) disclose that the

Table 1
Comparison of X_R with experiments

Case	ER	X_R/H_b (exp.)	X_R/H_b (linear)	X_R/H_b (nonlinear)
Driver and Seegmiller ($\alpha = 0$)	1.125	6.26 ± 0.10	6.21	6.30
Driver and Seegmiller ($\alpha = 6$)	1.125	8.30 ± 0.15	8.37	8.87
Eaton and Johnston	1.667	7.95 ± 0.30	7.90	7.97

zeroth-order EAHM gives a good agreement with the experiment. This is because the nonlinear straining effect of b_{ij} is explicitly incorporated into the heat flux model. As shown in Fig. 10(b), the wall heat transfer of the first-order EAHM is slightly lower than that of the zeroth-order EAHM. However, the prediction of the second-order EAHM lies between them. A closer inspection of Figs. 9 and 10 indicates that the straining effect in EAHM is critical to the constitutive relation of heat transfer. The contribution of the heat flux to the modeling is more significant than that of the nonlinear stress–strain relation.

5.4. Impinging jet flow

An impinging jet flow, despite its relatively simple geometry, exhibits extremly complex flow characteristics. Among others, the flow in stagnation region is nearly irrotational and there is a large total strain along the streamline. To predict the jet impingement accurately, the straining effects should be incorporated into the turbulence model (Craft et al., 1996; Durbin, 1996; Park and Sung, 2001). In the previous section, it is observed that the third-order strain terms have no meaningful improvement on the wall heat transfer rate. Therefore, the prediction of the nonlinear model is obtained by the present $\tau_{ij}^{\text{quadratic}}$. The profiles of the normalized mean velocity and Reynolds stress are shown in Fig. 11. The predicted results are compared with the experimental data of Cooper et al. (1993). In a global sense, all predictions are in good agreement with the experiment. The present model and the model of Craft et al. (1996) predict well the developing region, where the stagnation flow is transformed into a radial wall jet. However, the model of Craft et al. (1996) slightly underpredicts the normal stress. This may be caused by the fact that the anisotropy of their model is not fully resolved in the near-wall region, shown in Fig. 4. On the contrary, the present model reasonably resolves the near-wall behavior.

The influence of the truncated EAHM on the prediction of heat transfer is displayed in Fig. 12(a). These results are compared with the experimental data of Yan (1993) and the prediction of 'linear + EAHM'. Although some discrepancies are observed between experiment and computation, the agreement is generally satisfactory. It is seen that the discrepancy is attenuated in the downstream of the stagnation region. As shown in Fig. 12(a), the overprediction by the 'linear + zeroth EAHM' is seen in the stagnation region ($r/D \leqslant 3$). Compared with the 'quadratic + zeroth EAHM', this overprediction is improved by the nonlinear stress–strain relation. However,the difference between the truncated EAHMs is negligible, keeping the quadratic stress–strain relation. This means that if EASM is introduced to the stress–strain relation, the higher-order strain terms of EAHM have a small effect on wall heat transfer. This is consistent with the result of a backward-facing step flow. In

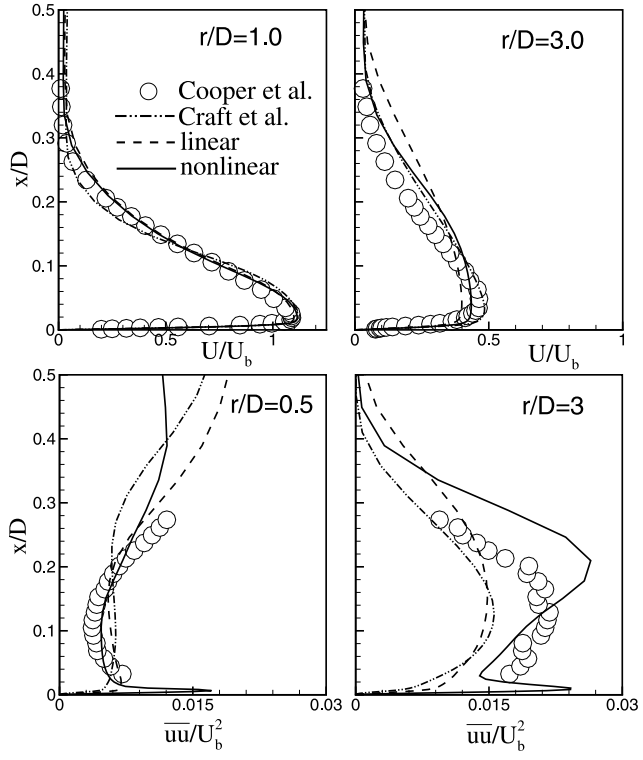

Fig. 11. Model comparisons of U/U_b and $\overline{uu}/U_b^2$ with experiment at $H/D = 2$ and $Re_D = 23,000$.

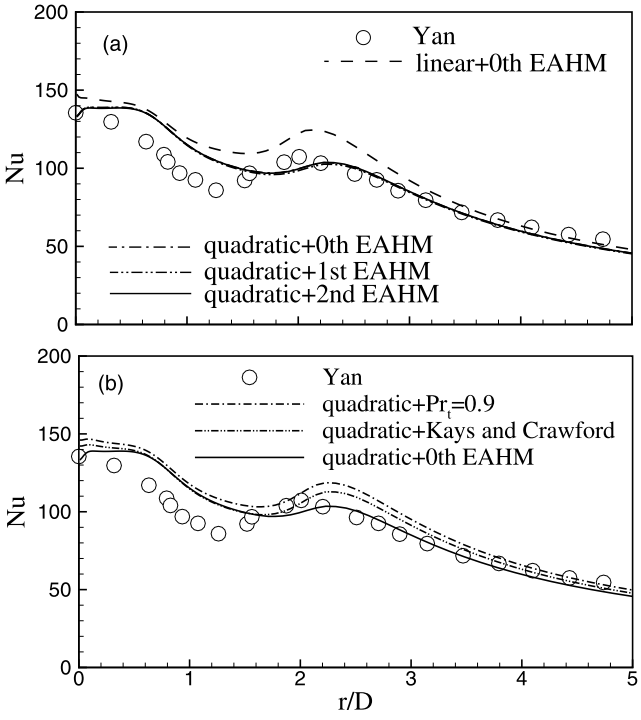

Fig. 12. Model comparisons of *Nu* with experiment.

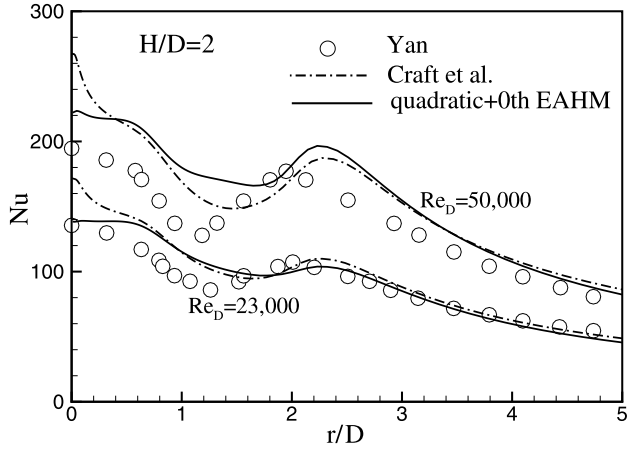

Fig. 13. Model comparisons of Nu with experiment.

order to evaluate the effect of Pr_t, a constant value of Pr_t and the formula of Kays and Crawford (1993) are employed. As seen Fig. 12(b), the model performances are marginal. However, the model of 'quadratic + zeroth EAHM' gives a slightly better agreement with the experimental data. Fig. 13 shows the model performance of the present 'quadratic + zeroth EAHM'. The result is compared with that predicted by the model of Craft et al. (1996). In the stagnation region, the present model prediction is better than the prediction by the model of Craft et al. (1996). Their overprediction may be attributed to the increasing behavior of anisotropy in the stagnation region. Examination of the present prediction with the experiment indicates that the anisotropy of Reynolds stresses is almost constant in the stagnation region. This suggests that the nonlinearity is small in the stagnation region. However, as shown in Fig. 2, the prediction by the model of Craft et al. (1996) exceeds the realizability limitation of the Reynolds stresses.

To examine the effect of the nozzle-to-wall distance H/D on heat transfer, several simulations are performed. Fig. 14 shows the stagnation Nu for various H/D. The standard k–ε model overpredicts for all H/D.

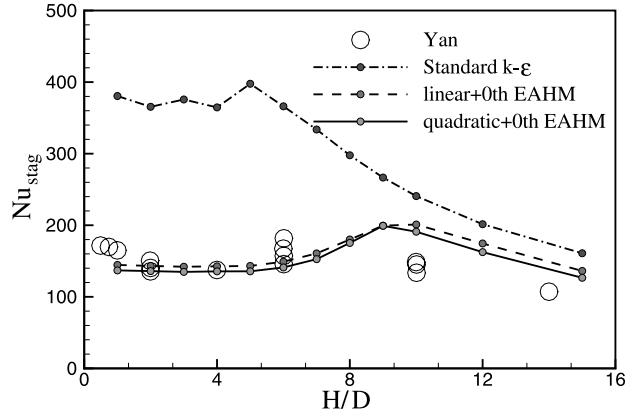

Fig. 14. Model comparisons of Nu_{stag} with experiment.

As H/D increases, the discrepency is attenuated, i.e., the effect of H/D is insignificant. However, the prediction by the present models is in good agreement with the experiment. Comparing with the prediction of the standard k–ε model and the present model, the eddy viscosity formula shows a important role for the prediction of Nu_{stag}. However, the present models show a similar distribution of Nu_{stag}. It is related that the nonlinearity is small in the stagnation region (Yan, 1993). The highest heat transfer rate is seen at $8 \leqslant H/D \leqslant 10$. These data can be useful in designing the heat transfer device pertinent to impinging jet flows.

6. Conclusions

The k–ε–f_μ model of Park and Sung (1997) has been extended to a nonlinear formulation for the prediction of turbulent flow and heat transfer in strongly non-equilibrium flows. A cubic EASM and a quadratic EAHM were developed on the basis of realizability constraints by using the Cayley–Hamilton theorem. In order to improve the near-wall behavior, the strain dependent coefficients were modified in a way similar to the general low-Reynolds-number model. To validate the model performance of the near-wall behavior, the present EASM was applied to a fully developed channel flow. The predicted results reproduced the wall behavior well. For separated and reattaching flows over a backward-facing step, the model performance of the strain dependent terms was examined with the truncated EASM and EAHM. It was found that the quadratic terms of the present EASM are dominant. The predicted results of EAHM indicated that the straining effect is critical to the constitutive relation of heat transfer. When EASM was introduced to the stress–strain relation, the role of the zeroth-order term was dominant compared to the first-order and second-order strain terms of EAHM. The validation of the model performance was extended to the heat transfer of impinging jet. Since the normal stress was almost constant in the stagnation region, the nonlinearity and the higher-order strain terms of EAHM had a small effect on heat transfer. The present EAHM showed a better prediction than the predictions by $Pr_t = 0.9$ and by the formula of Kays and Crawford. For various the nozzle-to-wall distance, the stagnation Nu showed the highest value at $8 \leqslant H/D \leqslant 10$. The thermal characteristics of impinging jet flow were well captured by the present model.

References

Abe, K., Kondoh, T., Nagano, Y., 1996. A two-equation heat transfer model reflecting second-moment closures for wall and free turbulent flows. Int. J. Heat Fluid Flow 17, 228–237.

Apsley, D.D., Leschziner, M.A., 1998. A new low-Reynolds-number nonlinear two-equation turbulence model for complex flows. Int. J. Heat Fluid Flow 19, 209–222.

Coleman, G.N., Mansour, N.N., 1992. Simulation and modeling of homogeneous compressible turbulence under isotropic mean compression. Turbulent Shear Flow 8, 269–282.

Craft, T.J., Launder, B.E., Suga, K., 1996. Development and application of a cubic eddy-viscosity model of turbulence. Int. J. Heat Fluid Flow 17, 108–115.

Driver, D.M., Seegmiller, H.L., 1985. Features of a reattaching turbulent shear layer in divergent channel flow. AIAA J. 163, 163–171.

Durbin, P.A., 1996. On the k–ε stagnation anomaly. Int. J. Heat Fluid Flow 17, 89–90.

Durbin, P.A., Laurence, D., 1996. Nonlocal effects in single point closure. In: Third Advances in Turbulence Research Conferencem, Korea University, Korea, pp. 109–120.

Eaton, J.K., Johnston, J.P., 1980. Turbulent Flow Reattachment: An Experimental Study of the Flow and Structure Behind a Backward-Facing Step, MD-39, Standard University.

Gatski, T.B., Speziale, C.G., 1993. On explicit algebraic stress models for complex turbulent flows. J. Fluid Mech. 254, 59–78.

Girimaji, S.S., 1996. Fully explicit and self-consistent algebraic Reynolds stress model. Theoret. Comput. Fluid Dyn. 8, 387–402.

Kasagi, N., Tomita, Y., Kuroda, A., 1992. Direct numerical simulation of passive scalar field in a turbulent channel flow. ASME J. Heat Transf. 114, 598–606.

Kays, W.M., Crawford, M.E., 1993. Convective heat and mass transfer, third ed. McGraw-Hill.

Launder, B.E., 1988. On the computation of convective heat transfer in complex turbulent flows. ASME J. Heat Transf. 110, 1112–1128.

Lee, M.J., Kim, J., Moin, P., 1990. Structure of turbulence at high shear rate. J. Fluid Mech. 216, 561–583.

Moser, R.D., Kim, J., Mansour, N.N., 1999. Direct numerical simulation of turbulent channel flow up to $Re_\tau = 590$. Phys. Fluids 11, 943–945.

Park, T.S., Sung, H.J., 1997. A new low-Reynolds-number k–ε–f_μ model for predictions involving multiple surfaces. Fluid Dyn. Res. 20, 97–113.

Park, T.S., 1999. Multigrid method and low-Reynolds-number k–ε model for turbulent recirculating Flows. Numer. Heat Transf., Part B: Fund. 36, 433–456.

Park, T.S., Sung, H.J., 1995. A nonlinear low-Reynolds-number k–ε model for turbulent separated and reattaching Flows—(I) flow field computation. Int. J. Heat Mass Transf. 38, 2657–2666.

Park, T.S., Sung, H.J., 2001. Development of a near-wall turbulence model and application to jet impingement heat transfer. Int. J. Heat Fluid Flow 22, 10–18.

Pope, S.B., 1975. A more effective-viscosity hypothesis. J. Fluid Mech. 72, 331–340.

Rhee, G.H., Sung, H.J., 2000. A nonlinear low-Reynolds-number heat transfer model for turbulent separated and reattaching Flows. Int. J. Heat Mass Transf. 43, 1439–1448.

Rogers, M.M., Mansour, N.N., Reynolds, W.C., 1989. An algebraic model for the turbulent flux of a passive scalar. J. Fluid Mech. 203, 77–101.

Shabany, Y., Durbin, P.A., 1997. Explicit algebraic scalar flux approximation. AIAA J. 35, 985–989.

Speziale, C.G., Gatski, T.B., 1997. Analysis and modelling of anisotropies in the dissipation rate of turbulence. J. Fluid Mech. 344, 155–180.

So, R.M.C., Sommer, T.P., 1996. An explicit algebraic heat-flux model for the temperature field. Int. J. Heat Mass Transf. 39, 455–465.

Speziale, C.G., Sarkar, S., Gatski, T.B., 1991. Modeling the pressure–strain correlation of turbulence: An invariant dynamical systems approach. J. Fluid Mech. 227, 245–272.

Tavoularis, S., Corrsin, S., 1981. Experiments in nearly homogeneous turbulent shear flow with a uniform mean temperature gradient. Part I. J. Fluid Mech. 104, 311–347.

Vogel, J.C., Eaton, J.K., 1985. Combined heat transfer and fluid dynamic measurements downstream of a backward-facing step. ASME J. Heat Transf. 107, 922–929.

Wallin, S., Johansson, A.V., 2000. An explicit algebraic reynolds stress model for incompressible and compressible turbulent flows. J. Fluid Mech. 403, 89–132.

Yan, X., 1993. A preheated-wall transient method using liquid crystals for the measurement of heat transfer on external surfaces and in ducts. PhD Thesis, University of California, Davis.